5. Lecture 5. Pointwise Error Control and Applications

In this lecture we extend the theory of Lecture 2 to the maximum norm following [38, 39]. We do this in sections 5.1 to 5.3. The maximum norm is of special interest in applications because it controls pointwise accuracy. We illustrate this in sections 5.4-5.7 for the simplest obstacle problem, which are based on [40, 39] Other Lebesgue norms can be dealt with similarly. In this lecture we assume, for simplicity, that the operator $\mathcal{L}$ is the Laplacian, so we study

$$-\Delta u = f \quad \text{in } \Omega, \qquad u = 0 \quad \text{on } \partial\Omega,$$

and consider polynomial degree $k = 1$. We point out that the convergence analysis as well as complexity are open questions in this setting.

5.1. **Error vs Residual.** We start by showing an error-residual relation different from, but equivalent to, that in (2.1). To this end we use the fact that the piecewise linear basis functions $\{\phi_z\}_{z\in\mathcal{N}_h}$ form a *partition of unity* of Ω:

$$\sum_{z\in\mathcal{N}_h} \phi_z = 1,$$

where $\mathcal{N}_h$ stands for all nodes of $\mathcal{T}_h$, including the boundary nodes. We denote by $\mathring{\mathcal{N}}_h$ the set of interior nodes. We have

$$\mathcal{B}[e_h,\psi] = \sum_{z\in\mathcal{N}_h} \mathcal{B}[e_h,\psi\phi_z] = \sum_{z\in\mathcal{N}_h} \int_{\omega_z} f\psi\phi_z + \int_{\gamma_z} J_h\psi\phi_z \qquad \forall \psi\in \mathring{H}^1(\Omega),$$

where $\omega_z = \operatorname{supp}(\phi_z)$ and γ_z are all the sides interior to ω_z, the so-called scheleton of the star (or patch) ω_z. Using Galerkin orthogonality (1.13), we arrive at

$$\begin{aligned} \mathcal{B}[e_h,v] &= \sum_{z\in\mathcal{N}_h} \int_{\omega_z} f(\psi-\bar\psi_z)\phi_z + \int_{\gamma_z} J_h(\psi-\bar\psi_z)\phi_z \\ &= \sum_{z\in\mathcal{N}_h} \int_{\omega_z} (f-\hat f_z)(\psi-\bar\psi_z)\phi_z + \int_{\gamma_z} J_h(\psi-\bar\psi_z)\phi_z. \end{aligned} \tag{5.1}$$

where $\bar\psi_z$ is the weighted L^2 projection of ψ over the constants on ω_z, $\bar\psi_z = 0$ for boundary nodes, and $\hat f_z$ is given by

$$\hat f_z := \frac{1}{2}\Big(\min_{\omega_z} f + \max_{\omega_z} f\Big).$$

This relation uncovers an intriguing property, namely that the jump residual dominates the interior residual. In fact the latter occurs here through data oscillation in the form $f - \hat f_z$.

Given $\varphi\in \mathring{H}^1(\Omega)\cap W_1^2(\Omega)$ and $\psi = \varphi - I_h\varphi$, the Bramble-Hilbert Lemma and *local second order* interpolation estimates for I_h given in (1.22) yield

$$\|\psi-\bar\psi_z\|_{0,1;\omega_z} \preccurlyeq h_z\|\nabla\psi\|_{0,1;\omega_z} = h_z\|\nabla(\varphi-\Pi_h\varphi)\|_{0,1;\omega_z} \preccurlyeq h_z^2\|D^2\varphi\|_{0,1;N(\omega_z)}$$

and, with the additional use of a scaled trace theorem,

$$\|\psi-\bar\psi_z\|_{0,1;\gamma_z} \preccurlyeq h_z^{-1}\|\psi-\bar\psi_z\|_{0,1;\omega_z} + \|\nabla\psi\|_{0,1;\omega_z} \preccurlyeq h_z\|D^2\varphi\|_{0,1;N(\omega_z)},$$

where $N(\omega_z)$ is a discrete neighborhood of ω_z. In view of (5.1), and the relation $\mathcal{B}[e_h,\psi] = \langle\mathcal{R}(u_h),\psi\rangle$, the last two estimates yield the following one:

$$|\langle\mathcal{R}(u_h),\,\varphi\rangle| \preccurlyeq \max_{z\in\mathcal{N}_h}\Big(h_z^2\|(f-\hat f_z)\,\phi_z\|_{0,\infty;\omega_z} + h_z\|J_h\,\phi_z\|_{0,\infty;\gamma_z}\Big)\,\|D^2\varphi\|_{0,1;\Omega}. \tag{5.2}$$

Analogously, one obtains

$$|\langle\mathcal{R}(u_h),\,\varphi\rangle| \preccurlyeq \Big(\sum_{z\in\mathcal{N}_h} h_z^p\|(f-\hat f_z)\,\phi_z\|_{0,p;\omega_z}^p + h_z\|J_h\,\phi_z\|_{0,p;\gamma_z}^p\Big)^{1/p}\|\nabla\varphi\|_{0,p';\Omega}, \tag{5.3}$$

where $p' = p/(p-1)$ is the dual exponent of $p\in[1,\infty)$. The proof of (5.2)-(5.3) is straightforward and is thus omitted.

5.2. **Generalized Green's Functions.** To prove an L^∞-estimate we first invoke the uniform cone property of Ω and find a ball $B \subset \Omega$ of radius $\rho = h_{\min}^\beta$ ($\beta \geq 1$ to be determined) such that $\operatorname{dist}(x_0, B) \preccurlyeq \rho$. We then introduce a regularized delta function δ supported in B

$$\int_B \delta = 1, \qquad 0 \leq \delta \leq C\rho^{-d},$$

and corresponding regularized Green's function $G \in \mathring{H}^1(\Omega)$ satisfying $-\Delta G = \delta$. The following a priori bound proved [18, 38] will be crucial in the subsequent discussion

$$\|D^2 G\|_{0,1;\Omega} \preccurlyeq |\log h_{\min}|^2.$$

5.3. **Pointwise A Posteriori Error Analysis.** To derive a pointwise error estimate we need to relate the value $e_h(x_0)$, where e_h attains a maximum, with the PDE. In this respect we have

$$e_h(x_1) = \int_\Omega e_h \delta = \mathcal{B}[e_h, G]$$

where $x_1 \in B$. We then have the following estimate.

Lemma 5.1 (Pointwise Upper Bound)**.** *There exists an interpolation constant C^*, solely depending on mesh regularity, such that*

$$\|u - u_h\|_{0,\infty;\Omega} \leq C^* |\log h_{\min}|^2 \max_{z \in \mathcal{N}_h} \eta_z \tag{5.4}$$

where $h_{\min} := \min_{z \in \mathcal{N}_h} h_z$ and η_z is the star-based residual indicator

$$\eta_z := h_z^2 \|(f - \hat{f}_z)\, \phi_z\|_{0,\infty;\omega_z} + h_z \, \|J_h\, \phi_z\|_{0,\infty;\gamma_z}. \tag{5.5}$$

Proof. We first apply the classical Hölder estimate of De Giorgi and Nash to deduce that $w = e_h \in C^{0,\alpha}(\Omega)$ for $\alpha = 1 - d/p > 0$ and $\|w\|_{C^{0,\alpha}(\Omega)} \preccurlyeq \|\mathcal{R}(u_h)\|_{-1,p;\Omega}$. Consequently, (5.3) yields

$$\|w\|_{C^{0,\alpha}(\Omega)} \preccurlyeq \Big(\sum_{z \in \mathcal{N}_h} \zeta_z^p \Big)^{1/p}$$

with

$$\zeta_z := h_z \, \|(f - \hat{f}_z)\, \phi_z\|_{0,p;\omega_z^+} + h_z^{1/p} \, \|J_h\, \phi_z\|_{0,p;\gamma_z^+}.$$

Hence

$$|w(x_0) - w(x_1)| \preccurlyeq |x_0 - x_1|^\alpha \|w\|_{C^{0,\alpha}(\Omega)} \preccurlyeq |x_0 - x_1|^\alpha \Big(\sum_{z \in \mathcal{N}_h} \zeta_z^p \Big)^{1/p}. \tag{5.6}$$

On the other hand, with the help of (5.2),

$$w(x_1) = \langle w, \delta \rangle = \langle \nabla w, \nabla G \rangle = \langle \mathcal{R}(u_h), G \rangle \preccurlyeq |\log h_{\min}|^2 \max_{z \in \mathcal{N}_h} \eta_z. \tag{5.7}$$

Fixing $p > d$ and choosing $\beta = \alpha^{-1}$, we deduce that

$$h_{\min}^{\alpha\beta} \zeta_z \preccurlyeq h_z \zeta_z \preccurlyeq \eta_z |\omega_z^+|^{1/p} \qquad \text{for all } z \in \mathcal{N}_h. \tag{5.8}$$

Since $|x_0 - x_1|^\alpha \preccurlyeq \rho^\alpha = h_{\min}$, combining (5.6) and (5.7) leads to (5.4). □

We conclude this section with a pointwise lower bound whose proof we leave as an exercise. The construction, described in [38], is a modification of that in Lemma 2.2 to account for the L^∞-norm.

Lemma 5.2 (Pointwise Lower Bound)**.** *There exists an interpolation constant C_*, solely depending on mesh regularity, such that*

$$C_* h_z \, \|J_h\, \phi_z\|_{0,\infty;\gamma_z} \leq \|u - u_h\|_{0,\infty;\omega_z} + h_z^2 \|(f - \hat{f}_z)\, \phi_z\|_{0,\infty;\omega_z}. \qquad \forall z \in \mathcal{N}_h \tag{5.9}$$

5.4. **Variational Inequalities.** Free boundary problems are ubiquitous in applications, from nonlinear elasticity and plasticity to fluids and finance [24, 30, 42]. The detection and accurate approximation of the free boundary is often a primary goal of the computation. There are, however, no results in the literature which provide a posteriori error estimates for interfaces. In case they are defined as level sets, then the mere control of the solution(s) does not yield in general control of the interfaces. We examine these issues below for the obstacle problem.

We first introduce the *continuous* obstacle problem. Let Ω be a bounded, polyhedral, not necessarily convex domain in $\mathbb{R}^d$ with $d \in \{1, 2, 3\}$. Let $f \in L^\infty(\Omega)$ be a load function, $\chi \in H^1(\Omega) \cap C^{0,\alpha}(\bar\Omega)$ be a lower obstacle, and $g \in H^1(\Omega) \cap C^{0,\alpha}(\bar\Omega)$ be a Dirichlet boundary datum with $0 < \alpha \leq 1$. Both χ and g satisfy the compatibility condition

$$\chi \leq g \quad \text{on } \partial\Omega.$$

Let $\mathcal{K}$ be the following non-empty, closed and convex subset of $H^1(\Omega)$:

$$\mathcal{K} := \{v \in H^1(\Omega) \mid v \geq \chi \text{ a. e. in } \Omega \text{ and } v = g \text{ on } \partial\Omega\}.$$

The variational formulation of the continuous obstacle problem reads as follows:

$$u \in \mathcal{K}: \qquad \langle \nabla u, \nabla(u - v)\rangle \leq \langle f, u - v\rangle \qquad \text{for all } v \in \mathcal{K}. \tag{5.10}$$

It is well known that (5.10) admits a unique solution u [30, Theorem 6.2], [24], [42], which is also Hölder continuous [23]. The latter implies that the *contact set*

$$\Lambda := \{u = \chi\} := \{x \in \Omega \mid u(x) = \chi(x)\}$$

and the *free boundary* or *interface*

$$\mathcal{F} := \partial\{u > \chi\} \cap \Omega$$

are closed in Ω. We are interested in the numerical study of these two sets. To this end, we first approximate u by means of finite elements (see section 5.5) and, later on, we construct appropriate a posteriori *barrier sets* depending on data and the finite element solution u_h (see section 5.7).

Crucial facts, such as the location of Λ, are encoded in the non-positive functional $\sigma \in H^{-1}(\Omega) = \mathring{H}^1(\Omega)^*$ defined by

$$\langle \sigma, \varphi\rangle = \langle f, \varphi\rangle - \langle \nabla u, \nabla\varphi\rangle \qquad \text{for all } \varphi \in \mathring{H}^1(\Omega), \tag{5.11}$$

which plays the role of a *multiplier* for the unilateral constraint. In fact, we have $\sigma = f + \Delta\chi$ in the interior of the contact set $\Lambda = \{u = \chi\}$, where σ is typically < 0, and $\sigma = 0$ in the open *non-contact* set $\Omega \setminus \Lambda = \{u > \chi\}$.

Let $\chi_h := I_h\chi$ be the discrete obstacle and let $I_h g$ be the discrete Dirichlet boundary datum. The discrete counterpart $\mathcal{K}_h$ of $\mathcal{K}$ is then

$$\mathcal{K}_h := \{v_h \in \mathbb{V}_h \mid v_h \geq \chi_h \text{ in } \Omega \text{ and } v_h = I_h g \text{ on } \partial\Omega\}.$$

Note that it is sufficient to check the unilateral constraint of $\mathcal{K}_h$ only at the nodes. The set $\mathcal{K}_h$ is non-empty, convex, closed but in general not a subset of $\mathcal{K}$ (non-conforming approximation). The *discrete* obstacle problem reads as follows:

$$u_h \in \mathcal{K}_h: \quad \langle \nabla u_h, \nabla(u_h - v_h)\rangle \leq \langle f, u_h - v_h\rangle \qquad \text{for all } v_h \in \mathcal{K}_h. \tag{5.12}$$

Problem (5.12) admits a unique solution (use [24], [30] in the Hilbert space $\mathbb{V}_h$).

To understand the issues involved in deriving sharp pointwise a posteriori error estimates, it is revealing to consider simple one-dimensional situations. We thus resort to Figures 5.1-5.3, which were produced with the estimators of this paper. These pictures display three meshes together with discrete solutions (thin lines). The forbidden region below χ is shaded for ease of visualization and χ_h is shown by thick lines. Our estimators control both errors $u - u_h$ in the maximum norm and $\sigma - \sigma_h$ in a negative Sobolev norm, which is altogether consistent with [47]. An *optimal* error estimator and associated adaptive procedure, such as those given in this paper, should exhibit the following basic properties:

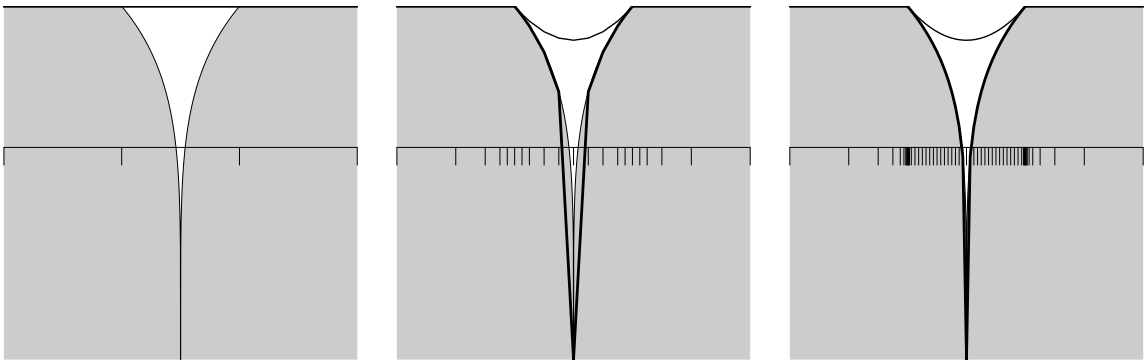

FIGURE 5.1. Localization for an obstacle with downward cusp

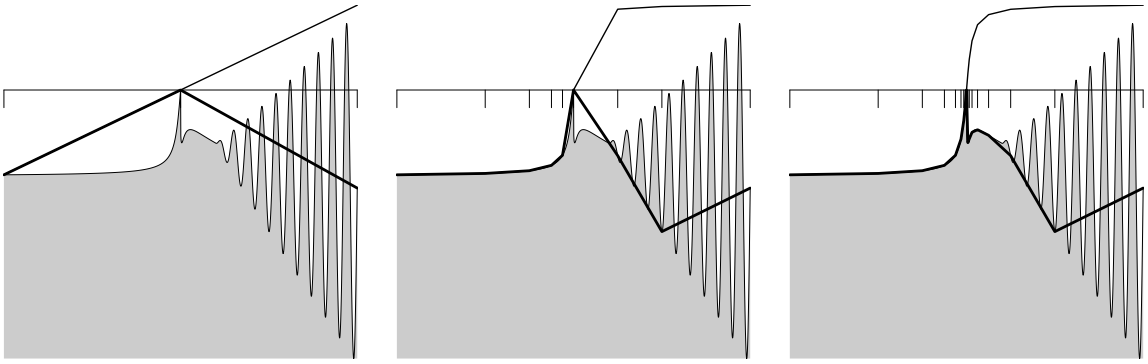

FIGURE 5.2. Localization for an oscillatory obstacle below u_h

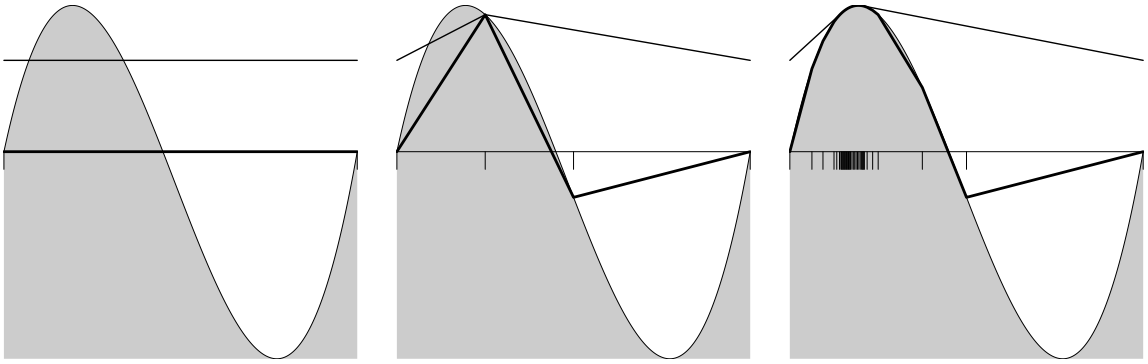

FIGURE 5.3. Localization for an obstacle not resolved on coarse grids

- In the discrete contact set $\{u_h = \chi_h\}$ the estimator must be insensitive (apart from oscillations) to the forcing term f, which should not dictate mesh quality. Figures 5.1 and 5.2 illustrate this property since the meshes are rather coarse in the contact sets.
- In the non-contact set $\{u_h > \chi_h\}$ the estimator must be insensitive to the obstacle and thus reduce to the usual estimator for the Laplacian. This effect is shown in Figures 5.1 and 5.2. The refinement in

Figure 5.1 is due to the curvature generated by $f=-1$ but not to the cusp of χ pointing downwards. On the other hand, the estimator does not feel the oscillatory character of χ in Figure 5.2 because it takes place below the discrete solution u_h. Overall there is an excellent accuracy for u in the non-contact set even though the approximation of χ is rather rough.

- The estimator must be able to detect the situation $\chi > u_h$, due to the nonconformity, and refine accordingly. This is depicted in Figure 5.3, where the concave part of χ above u_h is detected early on and thereby the solution is lifted up.
- If $\sigma = \Delta u + f$ happens to be singular with respect to the Lebesgue measure, as in Figure 5.1, then we could expect a strong refinement near the discrete free boundary. In fact, the piecewise linear approximation σ_h of σ cannot be very accurate in such a case no matter whether the corresponding singularity in the exact solution u can be resolved in the discrete space.
- It is not advisable to preadapt the mesh according to data f and χ since the contact set in unknown beforehand and its local mesh size should only depend on χ but not f, whereas the opposite situation occurs in the non-contact set.

5.4.1. *Discrete Full-contact Set and Multiplier.* We first introduce some notation. Let J_h be the jumps of the normal derivatives of u_h across interior sides (nodes/edges/faces in 1d/2d/3d, respectively). More precisely, given a common side S of two different simplices T^+ and T^-, we have on S

$$J_h = [\![\partial_n u_h]\!] = \left[\partial_n u_{h|T^+} - \partial_n u_{h|T^-}\right] \cdot n,$$

where n is the normal of S that points from T^- to T^+. We denote the union of all interior sides (inter-element boundaries) by Γ. For a node $z \in \mathcal{N}_h$, let $\omega_z = \operatorname{supp}(()\,\phi_z)$ be the finite element star and $\gamma_z = \Gamma \cap \operatorname{int} \omega_z$ be the union of all interior sides in ω_z. We define

$$\mathcal{C}_h = \{z \in \mathcal{N}_h \mid u_h = \chi_h \text{ and } f \le 0 \text{ in } \omega_z,\ J_h \le 0 \text{ on } \gamma_z\}$$

to be the set of *full-contact nodes* and denote by

$$\Omega_h^0 = \Big\{x \in \Omega \mid \sum_{z\in\mathcal{C}_h} \phi_z(x) = 1\Big\}, \qquad \Omega_h^+ = \Omega\backslash\Omega_h^0$$

the discrete *full-contact set* and its complement. Furthermore we set $\Gamma_h^0 = \Gamma \cap \Omega_h^0$ and $\Gamma_h^+ = \Gamma \cap \Omega_h^+$. We clearly have

$$z \in \mathcal{N}_h \setminus \mathcal{C}_h \implies \omega_z \subset \overline{\Omega_h^+} \text{ and } \gamma_z \subset \overline{\Gamma_h^+}. \tag{5.13}$$

Finally, let $\Pi_h : L_1(\Omega) \to \mathring{\mathbb{V}}_h$ be the interpolation operator of [14]; see also [41]. Such a Π_h is both *positivity preserving*, which helps construct $\sigma_h \le 0$, and *second order* accurate, which is crucial in dealing with the second order maximum norm error.

With these notations at hand, we define the *discrete multiplier* $\sigma_h \in H^{-1}(\Omega)$ by using the partition of unity $\langle \sigma_h, \varphi\rangle = \sum_{z\in\mathcal{N}_h} \langle \sigma_h, \varphi\,\phi_z\rangle$ and setting

$$\begin{aligned}\langle \sigma_h, \varphi\,\phi_z\rangle = &\int_{\Omega_h^0} f\,\varphi\,\phi_z + \int_{\Gamma_h^0} J_h\varphi\,\phi_z \\ &+ \int_{\Omega_h^+} f\,(\Pi_h\varphi)(z)\,\phi_z + \int_{\Gamma_h^+} J_h\,(\Pi_h\varphi)(z)\,\phi_z\end{aligned} \tag{5.14}$$

for all $z \in \mathcal{N}_h$ and $\varphi \in \mathring{H}^1(\Omega)$. Note that $\Pi_h\varphi$ is evaluated at the node z, and is thus a *constant* for each $z \in \mathcal{N}_h$. Therefore, (5.13) gives

$$z \in \mathcal{N}_h \setminus \mathcal{C}_h \implies \langle \sigma_h, \varphi\,\phi_z\rangle = (\Pi_h\varphi)(z)\,s_z, \tag{5.15}$$

where s_z is a *nodal* multiplier:

$$s_z := \int_\Omega f\,\phi_z + \int_\Gamma J_h\phi_z, \qquad z \in \mathcal{N}_h. \tag{5.16}$$

It satisfies $s_z \le 0$ whenever $z \in \mathring{\mathcal{N}}_h \cup \mathcal{C}_h$. This follows from the definition of $\mathcal{C}_h$, if $z \in \mathcal{C}_h$, and from utilizing $v_h = u_h + \phi_z \in \mathcal{K}_h$ in (5.12), if $z \in \mathring{\mathcal{N}}_h$.

Lemma 5.3. *The discrete multiplier σ_h satisfies $\sigma_h \le 0$.*

Proof. Let $\varphi \in \mathring{H}^1(\Omega)$ be non-negative. Since $\Pi_h\varphi \ge 0$ in Ω and $\Pi_h\varphi = 0$ on $\partial\Omega$, (5.15) implies $\langle \sigma_h,\, \varphi\,\phi_z\rangle \le 0$ for all $z \in \mathcal{N}_h \setminus \mathcal{C}_h$. On the other hand, if $z \in \mathcal{C}_h$, then $f \le 0$ in ω_z as well as $J_h \le 0$ on γ_z by definition, whence $\langle \sigma_h,\, \varphi\,\phi_z\rangle \le 0$ follows from (5.14). □

The multiplier σ_h is *not* a discrete function and is thus non-computable. In evaluating our error estimator, we will only make use of the nodal multipliers s_z for $z \in \mathring{\mathcal{N}}_h \cup \mathcal{C}_h$. The properties of these computable multipliers are closely related to properties of σ_h (see Proposition 5.5 below).

5.4.2. *Galerkin Functional: Definition and Properties.* We are now in the position to define the Galerkin functional $\mathcal{G}_h \in H^{-1}(\Omega)$, which plays the role of the residual for (unconstrained) equations; see [39, 47]:

$$\begin{aligned}\langle \mathcal{G}_h,\, \varphi\rangle &:= \langle \nabla(u-u_h),\, \nabla\varphi\rangle + \langle \sigma-\sigma_h,\, \varphi\rangle \\ &= -\langle \nabla u_h,\, \nabla\varphi\rangle + \langle f-\sigma_h,\, \varphi\rangle \qquad \text{for all } \varphi \in \mathring{H}^1(\Omega).\end{aligned} \tag{5.17}$$

Integrating by parts and employing the partition of unity $(\phi_z)_{z\in\mathcal{N}_h}$, we obtain

$$\begin{aligned}\langle \mathcal{G}_h,\, \varphi\rangle &= \int_\Omega f\,\varphi - \int_\Omega \nabla u_h \nabla\varphi - \langle \sigma_h,\, \varphi\rangle = \int_\Omega f\,\varphi + \int_\Gamma J_h\,\varphi - \langle \sigma_h,\, \varphi\rangle \\ &= \sum_{z\in\mathcal{N}_h}\Bigg\{ \int_\Omega f\,\varphi\,\phi_z + \int_\Gamma J_h\,\varphi\,\phi_z - \int_{\Omega_h^0} f\,\varphi\,\phi_z - \int_{\Gamma_h^0} J_h\,\varphi\,\phi_z \\ &\qquad\qquad - \int_{\Omega_h^+} f\,(\Pi_h\varphi)(z)\,\phi_z - \int_{\Gamma_h^+} J_h\,(\Pi_h\varphi)(z)\,\phi_z\Bigg\} \\ &= \sum_{z\in\mathcal{N}_h}\Bigg\{ \int_{\Omega_h^+} f\,[\varphi-(\Pi_h\varphi)(z)]\,\phi_z + \int_{\Gamma_h^+} J_h\,[\varphi-(\Pi_h\varphi)(z)]\,\phi_z\Bigg\} \\ &= \int_{\Omega_h^+} f\,\Big[\varphi - \sum_{z\in\mathcal{N}_h}(\Pi_h\varphi)(z)\,\phi_z\Big] + \int_{\Gamma_h^+} J_h\,\Big[\varphi - \sum_{z\in\mathcal{N}_h}(\Pi_h\varphi)(z)\,\phi_z\Big] \\ &= \int_{\Omega_h^+} f\,[\varphi-\Pi_h\varphi] + \int_{\Gamma_h^+} J_h\,[\varphi-\Pi_h\varphi].\end{aligned}$$

This expression shows the effect of *full localization* of the Galerkin functional to the set Ω_h^+. The construction of $\tilde\sigma_h$ in [39] leads merely to a *partial* localization. The full localization of σ_h defined by (5.14) is due to the notion of full-contact nodes, which was introduced in [22] so as to achieve full localization in the context of a first order estimator. In [22, Remark 4.5] one finds also an argument that the sign conditions on f and J_h in the definition of $\mathcal{C}_h$ are crucial.

To exploit further cancellation properties, we introduce the constant values

$$\bar\psi_z = \begin{cases} \Big(\int_{\Omega_h^+}\phi_z\Big)^{-1}\int_{\Omega_h^+}\psi\,\phi_z, & \text{if } \rho_z = 0,\\ 0, & \text{else,}\end{cases}$$

for all $z \in \mathcal{N}_h$ and $\psi \in L_1(\Omega)$, where

$$\rho_z := \int_{\Omega_h^+} f\,\phi_z + \int_{\Gamma_h^+} J_h\,\phi_z.$$

Note that, in view of (5.12) and (5.13), we certainly have $\rho_z = 0$ if $u_h(z) > \chi_h(z)$ and perhaps by chance otherwise. Setting $\psi := \varphi - \Pi_h\varphi$, employing again the partition of unity, and the fact that $\bar\psi_z\,\rho_z = 0$ we can rewrite $\langle \mathcal{G}_h,\, \varphi\rangle$ as follows:

$$\langle \mathcal{G}_h,\, \varphi\rangle = \sum_{z\in\mathcal{N}_h}\int_{\Omega_h^+} f\,[\psi-\bar\psi_z]\phi_z + \int_{\Gamma_h^+} J_h\,[\psi-\bar\psi_z]\,\phi_z.$$

For nodes $z \in \mathcal{N}_h$ with $\rho_z = 0$, the value $\bar{\psi}_z$ is the weighted L^2-projection of ψ to the constant functions on $\omega_z \cap \Omega_h^+$. Hence, we can subtract a constant from the element residual at these nodes without altering the expression. In particular, we can write

$$\langle \mathcal{G}_h, \varphi \rangle = \sum_{z \in \mathcal{N}_h} \int_{\omega_z^+} [f - \hat{f}_z]\, [\psi - \bar{\psi}_z] \phi_z + \int_{\gamma_z^+} J_h\, [\psi - \bar{\psi}_z]\, \phi_z, \tag{5.18}$$

where

$$\omega_z^+ = \omega_z \cap \Omega_h^+, \qquad \gamma_z^+ = \gamma_z \cap \Omega_h^+, \tag{5.19}$$

and

$$\hat{f}_z = \begin{cases} \frac{1}{2}\big(\min_{\omega_z^+} f + \max_{\omega_z^+} f\big), & \text{if } \rho_z = 0, \\ 0, & \text{else.} \end{cases} \tag{5.20}$$

This shows that only the *oscillation* $f - \hat{f}_z$ of the interior residual f enters in the estimators on all stars with $\rho_z = 0$ and not f itself.

5.4.3. *Galerkin Functional: Estimates.* In order to bound the pointwise error $\|u - u_h\|_{0,\infty;\Omega}$, we will need an estimate of $\mathcal{G}_h$ in the dual norm

$$\|\mathcal{G}_h\|_{-2,\infty;\Omega} := \sup\big\{ \langle \mathcal{G}_h, \varphi \rangle \mid \varphi \in \mathring{H}^1(\Omega) \cap W_1^2(\Omega) \text{ with } \|D^2 \varphi\|_{0,1;\Omega} \le 1 \big\}. \tag{5.21}$$

Since $\mathcal{G}_h$ plays a similar role to the residual $\mathcal{R}$ in the linear theory of section 5.3, we simply collect the estimates and refer to section 5.3 for the proofs.

Let $w \in \mathring{H}^1(\Omega)$ be the Riesz representation of $\mathcal{G}_h$,

$$w \in \mathring{H}^1(\Omega): \qquad \int_\Omega \nabla w \cdot \nabla \varphi = \langle \mathcal{G}_h, \varphi \rangle \quad \text{for all } \varphi \in \mathring{H}^1(\Omega). \tag{5.22}$$

The following estimate will be instrumental in section 5.5 and, compared with [39], it exhibits extra localization and cancellation of the element residual. This results mimics Lemma 5.1.

Lemma 5.4 (Properties of w)**.** *The function w is Hölder continuous and satisfies*

$$\|w\|_{0,\infty;\Omega} \preccurlyeq |\log h_{\min}|^2 \max_{z \in \mathcal{N}_h} \eta_z \tag{5.23}$$

where $h_{\min} := \min_{z \in \mathcal{N}_h} h_z$ and η_z is the star-based residual indicator

$$\eta_z := h_z^2 \|(f - \hat{f}_z)\, \phi_z\|_{0,\infty;\omega_z^+} + h_z\, \|J_h\, \phi_z\|_{0,\infty;\gamma_z^+}, \tag{5.24}$$

with ω_z^+, γ_z^+, and $\hat{f}_z$ defined in (5.19) *and* (5.20)*.*

5.5. **Error Analysis: Barriers and Localized Error Estimates.** We now introduce the continuous barriers u_* (lower) and u^* (upper), and derive a posteriori comparison estimates via the *continuous* maximum principle, thereby imposing no geometric constraints on the mesh. This is in striking contrast to existing a priori error analyses.

Given a function v, let $v^+ = \max(v, 0)$ denote its non-negative part.

Proposition 5.5 (Lower barrier)**.** *Let u_* be the function*

$$u_* := u_h + w - \|w\|_{0,\infty;\Omega} - \|g - I_h g\|_{0,\infty;\partial\Omega} - \|(u_h - \chi)^+\|_{0,\infty;\Lambda_h}, \tag{5.25}$$

where Λ_h is the contact set

$$\Lambda_h := \bigcup \{ \omega_z : z \in \mathring{\mathcal{N}}_h \cup (\mathcal{C}_h \cap \partial\Omega) \text{ and } s_z < 0 \} \tag{5.26}$$

with s_z defined in (5.16)*. Then u_* satisfies*

$$u_* \le u \qquad \text{in } \Omega.$$

Proof. We split the proof into four steps.

1. Since

$$(u_* - u)_{|\partial\Omega} \;\le\; (u_h - u)_{|\partial\Omega} - \|g - I_h g\|_{0,\infty;\partial\Omega} \;\le\; 0,$$

the function $v := (u_* - u)^+$ satisfies

$$v_{|\partial\Omega} = 0. \tag{5.27}$$

We want to show that $\|\nabla v\|_{0,2;\Omega} = 0$ and then use (5.27) to conclude that $v = 0$.

2. In view of (5.25), (5.22), (5.17), and $\sigma \le 0$, we can write

$$\begin{aligned} \|\nabla v\|^2_{0,2;\Omega} &= \int_\Omega \nabla(u_* - u)\cdot\nabla v = \int_\Omega \nabla(u_h - u)\cdot\nabla v - \int_\Omega \nabla w\cdot\nabla v \\ &= \langle \sigma - \sigma_h,\, v\rangle \le -\langle \sigma_h,\, v\rangle\,. \end{aligned} \tag{5.28}$$

It thus remains to show $\langle \sigma_h,\, v\rangle = 0$, i. e. $\langle \sigma_h,\, v\,\phi_z\rangle = 0$ for all $z \in \mathcal{N}_h$.

3. We now show that

$$s_z = 0 \text{ or } z \in (\mathcal{N}_h \cap \partial\Omega)\setminus \mathcal{C}_h \implies \langle \sigma_h,\, v\,\phi_z\rangle = 0.$$

First, consider $z \in \mathcal{C}_h$ with $s_z = 0$. By definition of $\mathcal{C}_h$, we have $J_h \le 0$ on γ_z and $f \le 0$ in ω_z. Hence,

$$0 = s_z = \int_{\omega_z} f\,\phi_z + \int_{\gamma_z} J_h\,\phi_z$$

implies in fact $J_h = 0$ on γ_z and $f = 0$ in ω_z. This yields

$$\begin{aligned} \langle \sigma_h,\, v\,\phi_z\rangle = &\int_{\omega_z\cap\Omega_h^0} f\,v\,\phi_z + \int_{\gamma_z\cap\Omega_h^0} J_h\,v\,\phi_z \\ &+ (\Pi_h v)(z)\left[\int_{\omega_z\setminus\Omega_h^0} f\,\phi_z + \int_{\gamma_z\setminus\Omega_h^0} J_h\phi_z\right] = 0. \end{aligned}$$

Next, for $z \in \mathcal{N}_h\setminus\mathcal{C}_h$ with $s_z = 0$, we directly obtain $\langle \sigma_h,\, v\,\phi_z\rangle = 0$ by (5.15). Finally, if $z \in (\mathcal{N}_h \cap \partial\Omega)\setminus\mathcal{C}_h$ is a boundary node not being in full-contact, then (5.15) and $(\Pi_h v)(z) = 0$ give $\langle \sigma_h,\, v\,\phi_z\rangle = 0$.

4. It remains to show that there is no node $z \in \mathring{\mathcal{N}}_h \cup \mathcal{C}_h$ with $\langle \sigma_h,\, v\,\phi_z\rangle < 0$ and $s_z < 0$. Suppose that z were such a node. Then there would exist an $x \in \omega_z$ with $v(x) > 0$, whence the definitions of u_* and Λ_h give

$$u_h(x) > u(x) + \|(u_h - \chi)^+\|_{0,\infty;\Lambda_h} \ge \chi(x) + \|(u_h - \chi)^+\|_{0,\infty;\omega_z} \ge u_h(x).$$

This contradiction concludes the proof. □

Proposition 5.6 (Upper barrier)**.** *The function*

$$u^* := u_h + w + \|w\|_{0,\infty;\Omega} + \|g - I_h g\|_{0,\infty;\partial\Omega} + \|(\chi - u_h)^+\|_{0,\infty;\Omega} \tag{5.29}$$

satisfies

$$u \le u^* \qquad \text{in } \Omega.$$

Proof. We proceed as in Proposition 5.5, dealing with $v := (u - u^*)^+ \in \mathring{H}^1(\Omega)$ and using $\sigma_h \le 0$ from Lemma 5.3. The crucial property $\langle \sigma,\, (u - u^*)^+\rangle = 0$ follows easily as in [39, Proposition 4.1]. □

Combining the results of Lemma 5.4 and Propositions 5.5 and **??**, we can now establish an upper a posteriori error estimate.

Theorem 5.7 (Reliability)**.** *Let (u, σ) be the continuous solution satisfying* (5.10) *and* (5.11)*, and let (u_h, σ_h) be the discrete solution satisfying* (5.12) *and* (5.14)*, respectively. Then the following global a posteriori upper bound holds:*

$$\max\left\{\|u - u_h\|_{0,\infty;\Omega}, \|\sigma - \sigma_h\|_{-2,\infty;\Omega}\right\} \le \mathcal{E}_h, \tag{5.30}$$

where $\|\cdot\|_{-2,\infty;\Omega}$ *is defined in* (5.21)*, the error estimator* $\mathcal{E}_h$ *is given by*

$$\begin{aligned}\mathcal{E}_h &:= C_*|\log h_{\min}|^2 \max_{z\in\mathcal{N}_h}\eta_z && \text{localized residual}\\ &\quad + \|(\chi-u_h)^+\|_{0,\infty;\Omega} + \|(u_h-\chi)^+\|_{0,\infty;\Lambda_h} && \text{localized obstacle approx.}\\ &\quad + \|g-I_hg\|_{0,\infty;\partial\Omega} && \text{boundary datum approx,}\end{aligned}$$

C_* *is twice the geometric constant hidden in* (5.23)*, solely depending on mesh regularity,* η_z *is the star-based indicator defined in* (5.24)*, and* Λ_h *is defined in* (5.26)*.*

Proof. Combining Propositions 5.5 and 5.6, we obtain $u_* \le u \le u^*$, whence

$$\|u-u_h\|_{0,\infty;\Omega} \le 2\|w\|_{0,\infty;\Omega} + \|(\chi-u_h)^+\|_{0,\infty;\Omega} + \|(u_h-\chi)^+\|_{0,\infty;\Lambda_h} + \|g-I_hg\|_{0,\infty;\partial\Omega}.$$

Lemma 5.4 then yields (5.30) for $u-u_h$. Finally, we resort to (5.17), namely,

$$\langle\sigma-\sigma_h,\,\varphi\rangle = \langle\mathcal{G}_h,\,\varphi\rangle + \langle u-u_h,\,\Delta\varphi\rangle \qquad \text{for all } \varphi\in\mathring{H}^1(\Omega)\cap W_1^2(\Omega),$$

and make use of (5.2) in conjunction with the bound above for $\|u-u_h\|_{0,\infty;\Omega}$ to derive the remaining estimate for $\sigma-\sigma_h$. □

The latter observation is important for the establishment of lower bounds and underlines the significance of the Galerkin functional. The global upper bound of Theorem 5.7 is of *optimal order* because the computable quantities therein are (locally) bounded by the combined error $\|u-u_h\|_{0,\infty;\Omega} + \|\sigma-\sigma_h\|_{-2,\infty;\Omega}$ and data approximation as follows.

Theorem 5.8 (Efficiency)**.** *The following local lower bounds hold for any* $z\in\mathcal{N}_h$ *and* $T\in\mathcal{T}_k$*:*

$$h_z\|J_h\phi_z\|_{0,\infty;\gamma_z^+} \preccurlyeq \|u-u_h\|_{0,\infty;\omega_z^+} + \|\sigma-\sigma_h\|_{-2,\infty;\omega_z^+} + h_z^2\|f-\hat f_z\|_{0,\infty;\omega_z^+},$$
$$\|I_hg-g\|_{0,\infty;T\cap\partial\Omega} \le \|u-u_h\|_{0,\infty;T}, \qquad \|(\chi-u_h)^+\|_{0,\infty;T} \le \|u-u_h\|_{0,\infty;T},$$

and, if $\omega_z\subset\Lambda_h$*,*

$$\begin{aligned}\|(u_h-\chi)^+\|_{0,\infty;\omega_z} \preccurlyeq \|u-u_h\|_{0,\infty;\omega_z} &+ \|\sigma-\sigma_h\|_{-2,\infty;\omega_z} + h_z^2\|f-\hat f_z\|_{0,\infty;\omega_z}\\ &+ \|(\chi_h-\chi)^+\|_{0,\infty;\omega_z} + \|\,[\![\partial_n\chi_h]\!]\,\|_{0,\infty;\gamma_z}.\end{aligned}$$

The proofs of these estimates are very similar to those of the corresponding lower bounds in [39, §6] and are therefore omitted. The efficiency predicted by these estimates is corroborated computationally in §5.6.

5.6. **Numerical Experiments I: Pointwise Error.** In this section we present a couple of insightful examples computed with the finite element toolbox ALBERTA of Schmidt and Siebert [43]. This code implements a bisection algorithm for refinement and thus guarantees mesh regularity.

The factor $C_*|\log h_{\min}|$ of Theorem 5.7 is in practice replaced by $C^* = 0.02$. This choice is consistent with (5.30) for meshes with reasonable shape-regularity and moderate $h_{\min}$. For the computation of the maximum norm, functions are evaluated at the element Lagrange nodes corresponding to polynomials of degree 7. The marking strategy for refinement is based on the maximum norm criterion.

5.6.1. *Madonna's Obstacle: Reliability and Efficiency.* Let $\Omega := (-1,1)^2$ and the obstacle χ be the upward cone with tip at $x_0 = (\frac{3}{8},\frac{3}{8})$ and slope $m = 1.8$:

$$\chi(x) = 1 - m|x-x_0|.$$

The exact solution is radially symmetric with respect to x_0, vanishes at $|x-x_0| = \frac{1}{m}$ and has a first order contact with the obstacle at $|x-x_0| = \frac{1}{2m}$; this corresponds to height $\frac{1}{2}$ (see Figure 5.4). The obstacle is thus singular within the contact set, due to the upward tip, which leads to local refinement. Several meshes are displayed in Figure 5.9 below.

Since we know the exact solution u, this example allows for a precise computational study of the estimator $\mathcal{E}_h$. Figure 5.5 displays both $\mathcal{E}_h$ and $\|u-u_h\|_{0,\infty;\Omega}$ versus the number of degrees of freedom (DOFs), and clearly demonstrates the equivalence between them. This result is consistent with Theorems 5.7 (reliability) and 5.8 (efficiency), and confirms their optimality.

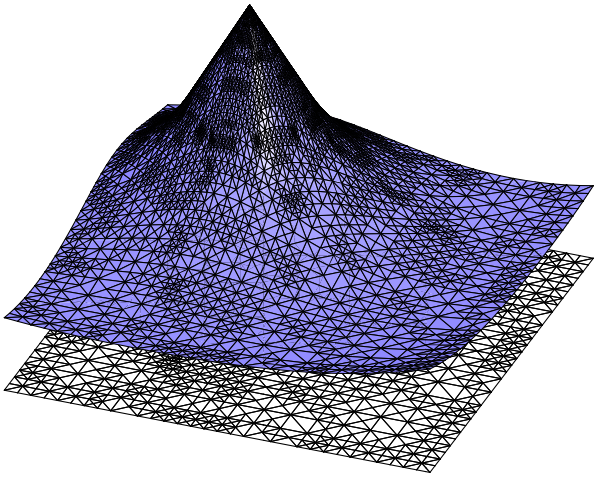

FIGURE 5.4. Madonna's obstacle: graph and grid of the discrete solution for adaptive iteration 14.

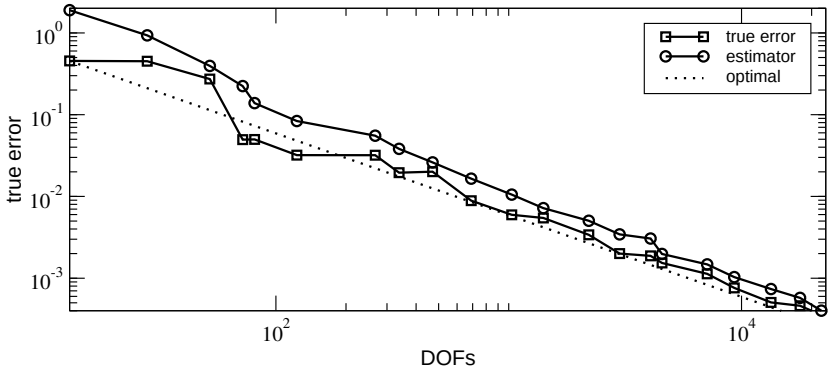

FIGURE 5.5. Madonna's obstacle: equivalence of estimator $\mathcal{E}_h$ and true pointwise error $\|u - u_h\|_{0,\infty;\Omega}$. The optimal decay is indicated by the dotted line with slope -1.

5.6.2. *Pyramid Obstacle: Full Localization.* We now consider the same pyramid obstacle as in [39, §7.4], namely

$$\chi(x) := \operatorname{dist}(x, \partial\Omega) - \tfrac{1}{5},$$

$f = -5$ and $g = 0$ on the square domain $\Omega := \{x \mid |x|_1 < 1\}$; see Figure 5.6. We show the dramatic effect of full localization of $\mathcal{E}_h$ in Figure 5.7, which exhibits coarse meshes within the full-contact set (bottom row) in striking contrast to recent results from [39] (top row). In addition, the new estimator is sharper with respect to the maximum norm than that in [39], and thus yields much fewer DOFs for about the same accuracy.

5.7. **Free Boundary Approximation: A Posteriori Barrier Sets.** The error in the approximation of σ is related to some 'weak distance' of the exact contact set Λ and an appropriate approximation; cf. [47, Remark 3.2]. However, the fact that the estimator $\mathcal{E}_h$ controls the pointwise error $\|u - u_h\|_{0,\infty;\Omega}$ allows in certain situations for more accurate *a posteriori* information on Λ and also on the exact free boundary (or interface) $\mathcal{F}$. This topic is the main concern of this section.

We consider the situation when one knows $\lambda > 0$ such that

$$\langle f, \varphi\rangle - \langle \nabla\chi, \nabla\varphi\rangle \;\le\; -\lambda \int_\Omega \varphi \tag{5.31}$$

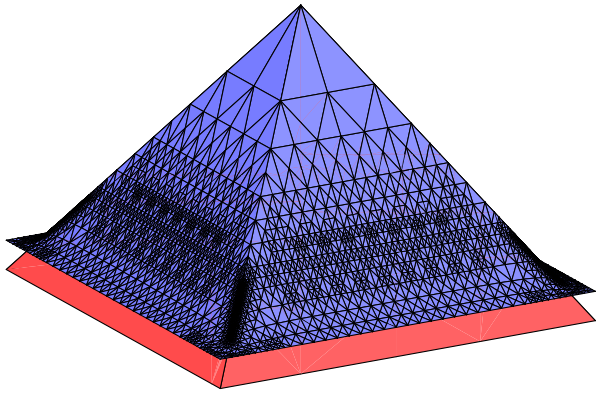

FIGURE 5.6. Pyramid obstacle: graph with grid of the discrete solution over the obstacle for adaptive iteration 10, displaying lack of refinement along the diagonals inside the full-contact set (effect of full localization).

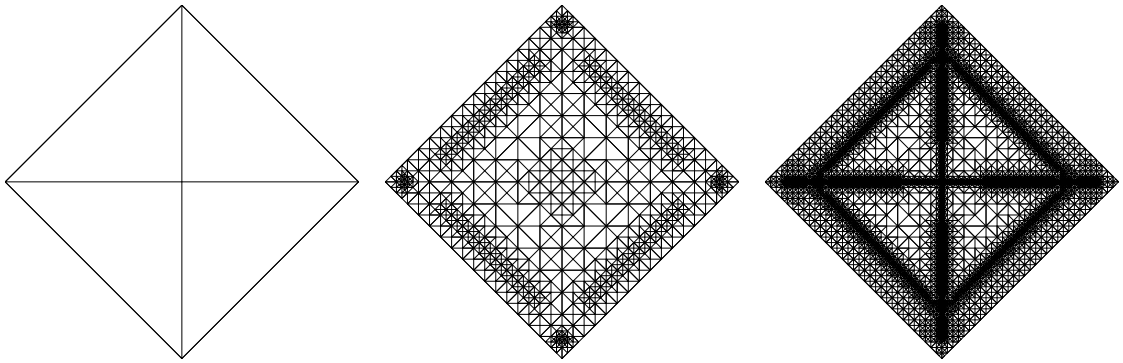

FIGURE 5.7. Pyramid obstacle: Comparison of grids obtained with the partially localized estimator of [39] (top) and the fully localized estimator (bottom). The meshes on the same column correspond to about the same value of the estimator, whereas the number of degrees of freedom (DOFs) are much reduced with the new approach. The benefits of full localization are apparent since the refinement on the diagonals in contact is avoided.

for all $\varphi \in \mathring{H}^1(\Omega)$ with $\varphi \geq 0$. Condition (5.31) guarantees *stability* of the exact free boundary $\mathcal{F}$ and is due to Caffarelli [12]; see also [24, §2.10]. Moreover, (5.31) implies

$$\sup_{B(x;r)} (u - \chi) \geq u(x) - \chi(x) + \frac{\lambda r^2}{2d} \tag{5.32}$$

for any $x \in \overline{\{u > \chi\}}$ and any $r > 0$ such that $B(x;r) \subset \Omega$. Its proof proceeds along the same lines as that of Lemma 3.1 in [24, Chapter 2].

Let us define $K := \{\operatorname{dist}(\cdot, \partial\Omega) \geq r_h\}$ and the *barrier sets*

$$\Lambda^* := \{u_h \leq \chi + \mathcal{E}_h\}, \qquad \Lambda_* := \Big\{\operatorname{dist}\big(\cdot, \{u_h \geq \chi_h + \mathcal{E}_h\}\big) \geq r_h\Big\}, \tag{5.33}$$

where

$$r_h^2 := \frac{2d}{\lambda}\big(2\mathcal{E}_h + \|(\chi_h - \chi)^+\|_{0,\infty;\{u_h \leq \chi_h + \mathcal{E}_h\}}\big). \tag{5.34}$$

The following result, based on Theorem 5.7 and (5.32), locates the exact contact set Λ and the free boundary $\mathcal{F}$ a posteriori.

Theorem 5.9 (A posteriori control of contact set and interface)**.** *The set Λ^* is an upper barrier set for the exact contact set $\Lambda = \{u = \chi\}$, i. e. $\Lambda \subset \Lambda^*$.*

Moreover, if the stability condition (5.31) *holds, then the set Λ_* is a lower barrier set for Λ in the sense that $\Lambda_* \cap K \subset \Lambda \cap K$, whence*

$$\mathcal{F} \cap K \subset \big(\Lambda^* \cap K\big) \setminus \operatorname{int}\big(\Lambda_* \cap K\big).$$

Remark 5.10 (Conditioning)**.** *In the light of* (5.32)*, λ dictates the quadratic growth of $u - \chi$ in the non-contact set away from the free boundary $\mathcal{F}$ and so: the larger λ the more stable $\mathcal{F}$, that is λ acts as a measure of conditioning of the free boundary. Correspondingly, the thicknesses of the strips $\Omega \setminus K$ and $\big(\Lambda^* \cap K\big) \setminus \operatorname{int}\big(\Lambda_* \cap K\big)$ depend inversely on λ.*

Remark 5.11 (Existence of exact interface)**.** *Suppose that condition* (5.31) *holds. Then $\Lambda_* \cap K \neq \emptyset$ implies $\Lambda \neq \emptyset$. Moreover, $\Lambda_* \cap K \neq \emptyset$ and $\Omega \setminus \Lambda^* \neq \emptyset$ imply $\mathcal{F} \neq \emptyset$.*

Proof of Theorem 5.9. We first prove $\Lambda \subset \Lambda^*$. We use Theorem 5.7 with $x \in \Lambda$

$$u_h(x) = u(x) + \big[u_h(x) - u(x)\big] \leq \chi(x) + \mathcal{E}_h$$

to deduce $x \in \Lambda^*$. We next prove $\Lambda_* \cap K \subset \Lambda \cap K$ provided that (5.31) holds. Let $x \in \Lambda_* \cap K$ and suppose that

$$u(x) > \chi(x). \tag{5.35}$$

Then, the definition of Λ_* in (5.33) implies that

$$u_h \leq \chi_h + \mathcal{E}_h \qquad \text{in } \overline{B(x;r_h)} \tag{5.36}$$

holds and (5.32) yields

$$\sup_{B(x;r_h)} (u - \chi) > \frac{\lambda r_h^2}{2d}. \tag{5.37}$$

Consequently, Theorem 5.7, (5.34), and (5.37) give for some point $y \in \overline{B(x;r_h)}$:

$$\begin{aligned} u_h(y) &= u(y) + \big[u_h(y) - u(y)\big] > \chi(y) + \frac{\lambda r_h^2}{2d} - \mathcal{E}_h \\ &= \chi(y) + 2\mathcal{E}_h + \|(\chi_h - \chi)^+\|_{0,\infty;\{u_h \leq \chi_h + \mathcal{E}_h\}} - \mathcal{E}_h \geq \chi_h(y) + \mathcal{E}_h. \end{aligned}$$

This contradicts (5.36) and so (5.35) is false. Consequently, $x \in \Lambda$ as asserted. □

Remark 5.12 (Estimate in distance)**.** *We stress that Theorem 5.9 relies solely on* (5.32) *and not on estimating the measure of* $\{0 < u - \chi < \epsilon\}$*, the so-called* non-degeneracy property *of Caffarelli* [12]*. This leads, in the* a priori *error analysis for* $\chi = \chi_h$*, to estimates in measure for the discrete free boundary relative to* $\mathcal{F}$ [6, 36]*. Bounds in distance require regularity of* $\mathcal{F}$ [6, 19, 36]*. We locate here* $\mathcal{F}$ *relative to*

$$\mathcal{F}_h = \partial\{u_h > \chi_h + \mathcal{E}_h\} \cap \Omega.$$

This dual approach yields estimates in distance *without regularity assumptions on the exact free boundary* $\mathcal{F}$*.*

Remark 5.13 (Computation of effective condition number)**.** *Statement* (5.36) *reveals that* (5.31) *is needed in the proof of Theorem 5.9 only for positive test functions* φ *with* $supp\,(\varphi) \subset \{u_h \le \chi_h + \mathcal{E}_h\}$*. Therefore, if* $\chi \in H^2(\Omega)$*, one can adaptively compute the condition number* λ *by*

$$\lambda = - \sup_{\{u_h \le \chi_h + \mathcal{E}_h\}} (f + \Delta\chi).$$

5.8. **Numerical Experiments II: Free Boundaries.** In this section we present several numerical experiments illustrating the impact of the a posteriori barrier sets in §5.7 on the numerical study of exact free boundaries.

5.8.1. *Madonna's Obstacle: Reliability and Efficiency.* Let us reconsider the example from §5.6.1, this time focusing on the approximation of the exact free boundary $\mathcal{F} = \{x \in \Omega \mid |x - x_0| = \frac{1}{2m}\}$. The condition number λ which enters the definition of r_h in (5.34), and thus the one of Λ_*, is computed according to Remark 5.13. Figure 5.8 depicts the true distance $\mathrm{dist}(\mathcal{F}, \mathcal{F}_h)$ between $\mathcal{F}$ and $\mathcal{F}_h = \partial\{u_h > \chi_h + \mathcal{E}_h\}$ together with r_h versus the number of DOFs; the number r_h essentially measures the gap between the two barrier sets. Both quantities decay with optimal order. Their behavior corroborates the reliability statement of Theorem 5.9 and, furthermore, reveals nice efficiency properties of r_h, which are not explained by the theory of section 5.7. Note also that, for the final computations the two barrier sets are quite close: $r_h \approx 0.02$. The grids and interface barriers in Figure 5.9 illustrate different stages in the information about the exact free boundary: the very coarse grid of the first column only indicates a possible exact free boundary; the still quite coarse grid of the second column assures the existence of the free boundary within the a posteriori annulus $\Lambda^* \backslash \Lambda_*$ (see Remark 5.11), and suggests that it might be a circle; the latter is further confirmed by the finer grid of the third column and corresponding better interface resolution.

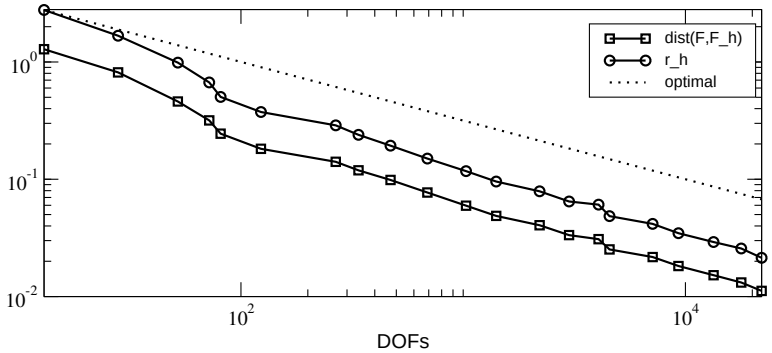

FIGURE 5.8. Madonna's obstacle: equivalence of $\mathrm{dist}(\mathcal{F}, \mathcal{F}_h)$ and the distance r_h of the barriers. The optimal decay is indicated by the dotted line with slope $-1/2$.

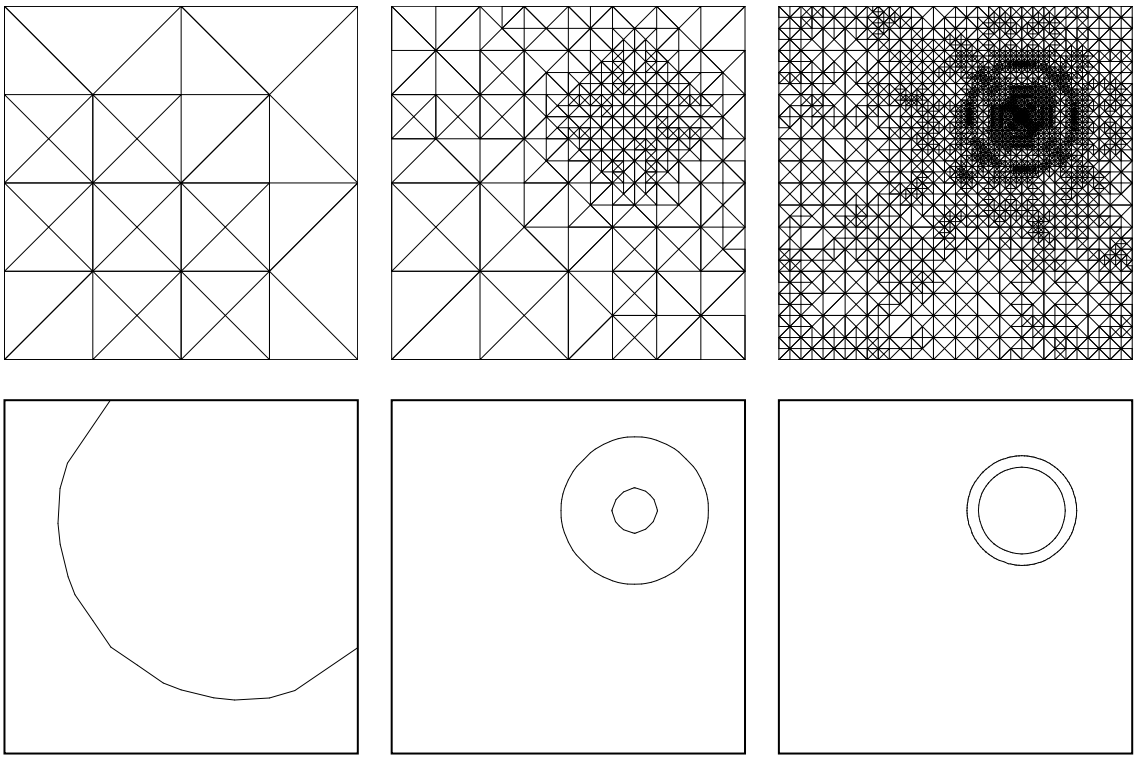

FIGURE 5.9. Madonna's obstacle: grids and interface barriers obtained by the adaptive algorithm in steps 1, 6, and 13.

5.8.2. *From Balls to Bones.* We consider the domain $\Omega = (-2,2) \times (-1,1)^{d-1}$, boundary value $g = 0$, several constant loads f, and the smooth obstacle

$$\chi(x) = \alpha - \beta(x_1^2 - 1)^2 - \gamma(|x|^2 - x_1^2) \tag{5.38}$$

with $\alpha = 10$, $\beta = 6$, $\gamma = 20$ in 2d, and $\alpha = 5$, $\beta = 6$, and $\gamma = 30$ in 3d. In 2d the graph of the obstacle consists of two hills connected by a saddle.

Tolerance	Interval for f_{crit}
$\tau \approx 0.5$	$(-3.3, -17.0)$
$\tau \approx 0.1$	$(-5.1, -9.5)$
$\tau \approx 0.05$	$(-5.5, -8.8)$
$\tau \approx 0.01$	$(-5.9, -8.1)$
$\tau \approx 0.005$	$(-6.0, -7.3)$
$\tau \approx 0.001$	$(-6.5, -6.9)$

Tolerance	Interval for f_{crit}
$\tau \approx 0.5$	$(-8.0, -21.0)$
$\tau \approx 0.25$	$(-8.5, -15.1)$
$\tau \approx 0.1$	$(-9.3, -13.9)$

TABLE 5.1. From balls to bones: A posteriori control of the interval containing f_{crit} for different tolerances in 2d (left) and 3d (right).

In what follows, "barrier sets for tolerance $\approx \tau$" (> 0) denote those barrier sets which are constructed in the first adaptive iteration with $\mathcal{E}_h \leq \tau$. The left column in Figure 5.10 illustrates the interface barriers for four constant loads $f = 0, -5.9, -8.1, -15$ in 2d for about the same tolerance $\tau \approx 0.01$; the exterior curves correspond to $\partial\Lambda^*$ whereas the interior curves display $\partial\Lambda_*$. For $f = 0$, the contact set does not contain the saddle, whereas, for $f = -15$, it does. This happens because the solution, being

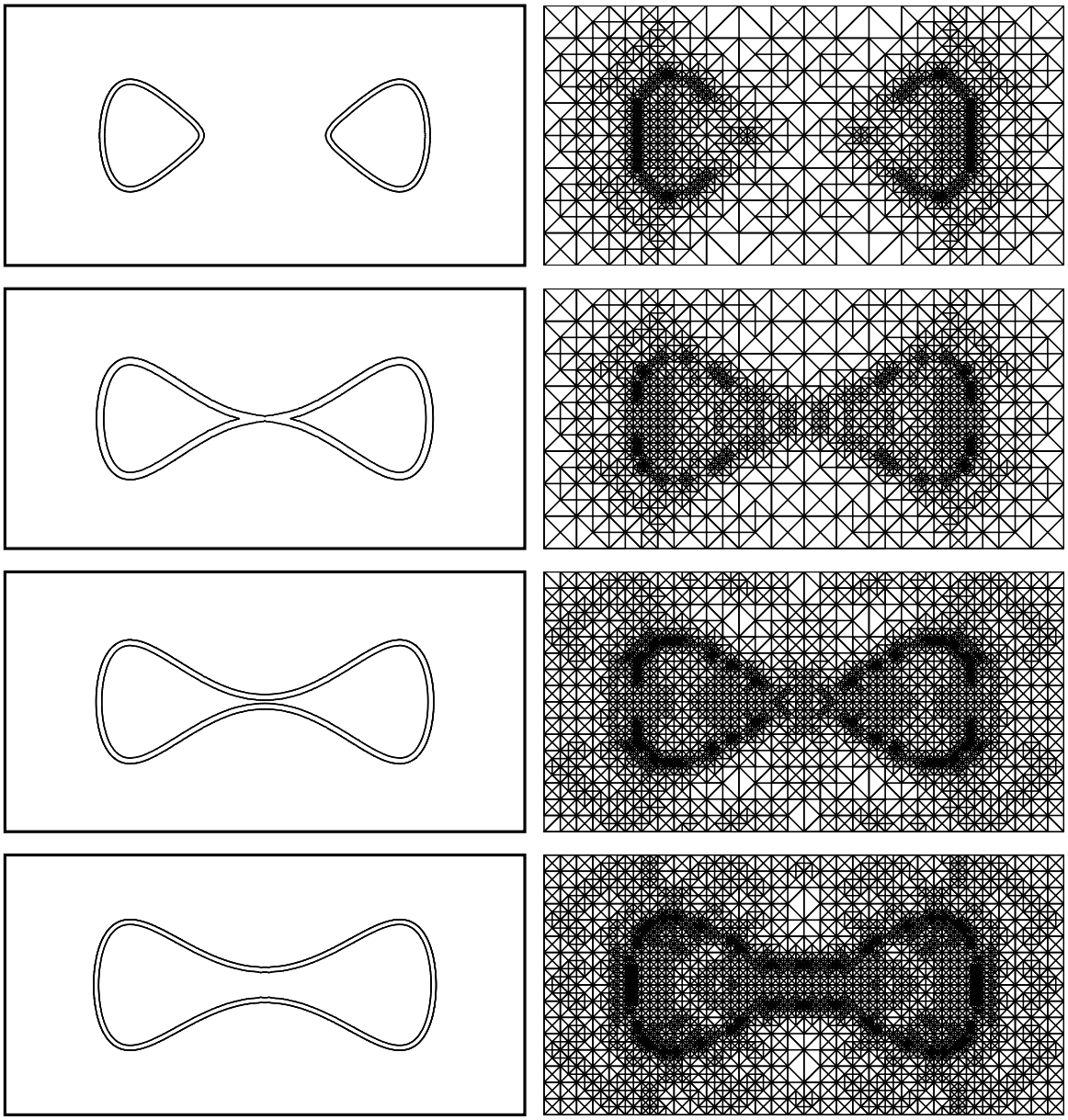

FIGURE 5.10. From balls to bones: Interface barriers for tolerance ≈ 0.01 (left) and adaptive grids for tolerance ≈ 0.15 (right) in 2d for forcing term $f = 0, -5.9, -8.1, -15$ (from top to bottom). The distance of the barriers is ≈ 0.05 for all four forces.

pushed down by f, adheres longer to the obstacle. During the transition between these two extreme cases, the free boundary has a singular point, namely a "double-cusp" at the origin, for some critical value $f_{\rm crit}$. The barrier sets constructed in section 5.7 from the discrete solution and the estimator give a reliable range for $f_{\rm crit}$: as long as Λ^* does not contain the saddle and $\Lambda_* \neq \emptyset$, the true contact set Λ exists and does not contain the saddle; this happens for $0 \geq f > -5.9$. For $f < -8.1$, the lower barrier Λ_* contains the saddle and exhibits a dumbbell shape, and so does Λ; hence, $f_{\rm crit} \in (-5.9, -8.1)$. The size of this interval depends on the size of the estimator $\mathcal{E}_h$ and decreases for smaller values of $\mathcal{E}_h$, as documented in Table 5.1. Although the true interface develops a singularity, it is worth noticing

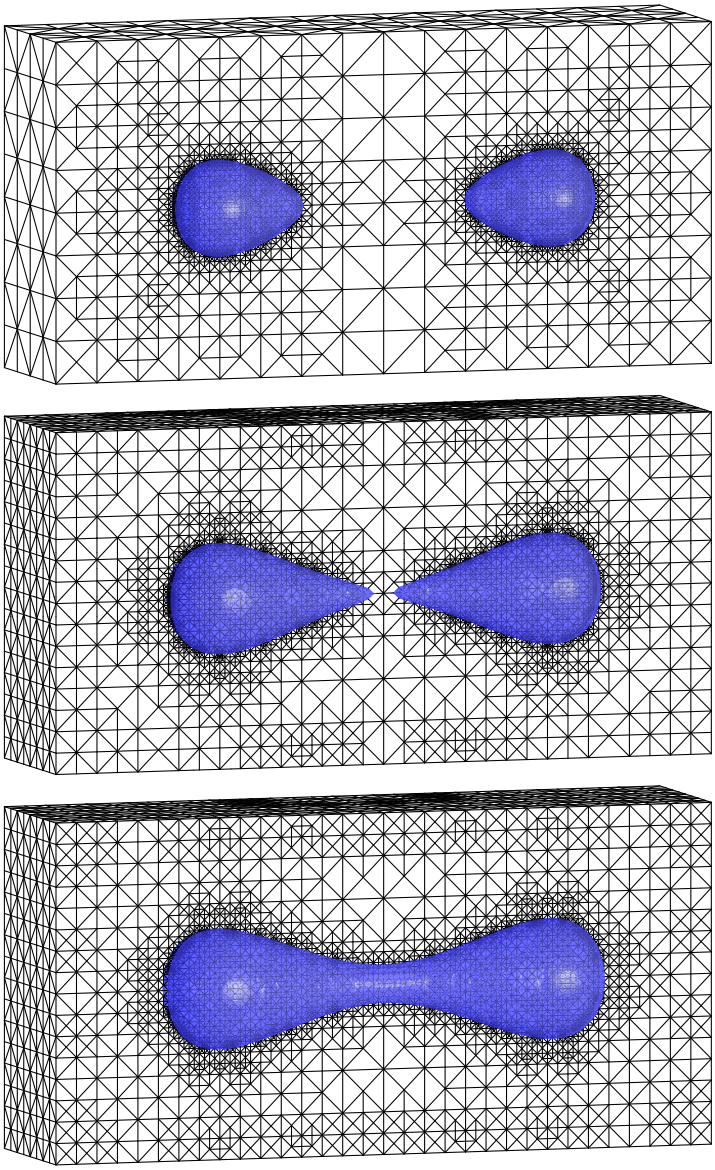

FIGURE 5.11. From balls to bones: Upper barrier $\partial\Lambda^* \cap \Omega$ and adaptive grids in 3d for tolerance ≈ 0.25 and $f = 0, -9.3, -13.9$. The distance of the barriers is ≈ 0.1 for all three forces.

that $u \in W^2_\infty(\Omega)$ and thus no special refinement is needed to approximate either u (or σ). Moreover, $f + \Delta\chi \leq -16$ in Ω for the 4 loads, which shows that the double-cusp is not due to lack of stability. The interface estimate of Theorem 5.9 thus applies and provides a posteriori error control of the entire free boundary including the double-cusp.

A similar situation occurs in 3d, as depicted in Figure 5.11, for tolerance ≈ 0.25 and values $f = 0, -9.3, -13.9$. These pictures as well as Figure 5.4 were created using the graphics package GRAPE [27]. For tolerance ≈ 0.25, we can predict that a double-cusp forms for $f_{\text{crit}} \in (-9.3, -13.9)$. The interval for other tolerances is shown in Table 5.1.

5.9. **Exercises.**

5.9.1. *Exercise: The Logarithmic Factor.* Let $-\Delta G = \delta_{x_0}$ be the Green's function satisfying $G = 0$ on $\partial\Omega$. Prove that

$$\|\nabla(G - G_h)\|_{L^1(\Omega)} \geq \inf_{\varphi \in \mathbb{V}_h} \|\nabla G - \varphi\|_{L^1(\Omega)} \geq Ch|\log h|,$$

where $\mathbb{V}_h$ is the space of piecewise constant vector-valued functions over $\mathcal{T}_h$. This partially explains the presence of a logarithmic factor in the maximum norm error estimates, which is due to the fact that P^1 finite elements cannot approximate the Green's function singularity with optimal accuracy. Hint: Decompose $\mathcal{T}_h$ into the disjoint sets $A_i := \{T \in \mathcal{T}_h : ih \leq \text{dist } (T, x_0) < (i+1)h\}$, use the properties $|D^2 G(x)| \approx 1/|x - x_0|^n$ and $|D^3 G(x)| \approx 1/|x - x_0|^{d+1}$, and Taylor's formula within each element $T \in A_i$ to estimate $\nabla G - \varphi$; here $\approx$ means equivalence. Upon realizing that card $(A_i) \leq Ci^{d-1}$, add on i.

5.9.2. *Exercise: Star Estimator.* Derive an H^1 upper a posteriori error estimate in terms of star estimators such as η_z.

5.9.3. *Exercise: Positivity Preserving Interpolation.* The construction of the operator Π_h is rather tricky snce the usual interpolation operators of Clement and Scott-Zhang do not preserve positivity. Given an interior node $z \in \mathring{\mathcal{N}}_h$, let B_z be the largest ball contained in ω_z. Given a function $v \geq 0$ let

$$v_z = \frac{1}{|B|} \int_B v,$$

and

$$\Pi_h v := \sum_{z \in \mathring{\mathcal{N}}_h} v_z \phi_z.$$

Show that $\Pi_h v \geq 0$, that Π_h is a local operator, and that (1.22) is valid with $t = 0, 1$ and $s = 2$.

References

[1] M. Ainsworth and J.T. Oden, *A Posteriori Error Estimation in Finite Element Analysis*, John Wiley & Sons, Inc., 2000.

[2] E. Bänsch, *Local mesh refinement in 2 and 3 dimensions*, Impact Comput. Sci. Engrg., 3 (1991), 181–191.

[3] E. Bänsch, P. Morin, and R.H. Nochetto, *An adaptive Uzawa FEM for the Stokes problem: Convergence without the inf-sup condition*, SIAM J. Numer. Anal. (2002).

[4] P. Binev, W. Dahmen, and R. DeVore, *Adaptive finite element methods with convergence rates*, Numer. Math., 97 (2004), 219–268.

[5] P. Binev, W. Dahmen, R. DeVore, and P. Petruchev, *Approximation classes for adaptive methods*, Serdica Math. J., 28 (2002), 391–416.

[6] F. Brezzi and L. A. Caffarelli, *Convergence of the discrete free boundaries for finite element approximations*, RAIRO Numer. Anal., 17 (1983), pp. 385–395.

[7] F. Brezzi and M. Fortin, *Mixed and Hybrid Finite Element Methods*, Springer-Verlag, 1991.

[8] S.C. Brenner and L.R. Scott, *The Mathematical Theory of Finite Elements*, Springer (2002), 2nd ed.

[9] C. Carstensen, R. Verfürth, *Edge residuals dominate a posteriori error estimates for low order finite element methods*, SIAM J. Numer. Anal., 36 (1999), 1571–1587.

[10] J.M. Cascón and R.H. Nochetto, *Convergence and optimal complexity of AFEM for general elliptic PDE and applications*, (to appear).

[11] J.M. Cascón, R.H. Nochetto, and K. Siebert, *Design and convergence of an AFEM in H(div)*, (to appear).

[12] L. A. Caffarelli, *A remark on the Hausdorff measure of a free boundary, and the convergence of coincidence set*, Boll. Unione Mat. Ital., V. Ser., A 18 (1981), pp. 109–113.

[13] Z. Chen and F. Jia, *An adaptive finite element algorithm with reliable and efficient error control for linear parabolic problems*, Math. Comp., 73 (2004), 1163-1197.

[14] Z. Chen and R. H. Nochetto, *Residual type a posteriori error estimates for elliptic obstacle problems*, Numer. Math., 84 (2000), pp. 527–548.

[15] Ph. Ciarlet, *The Finite Element Method for Elliptic Problems.*, North-Holland, Amsterdam, 1978.

[16] S. Dahlke, W. Dahmen and K. Urban, *Adaptive wavelet methods for saddle point problems - Optimal convergence rates*, preprint.

[17] S. Dahlke, R. Hochmuth and K. Urban, *Adaptive wavelet methods for saddle point problems*, M2AN, 34, No. 5, 1003-1022 (2000).

[18] E. Dari, R. G. Durán, and C. Padra, *Maximum norm error estimators for three-dimensional elliptic problems*, SIAM J. Numer. Anal., 37 (2000), pp. 683–700.

[19] K. Deckelnick and K. G. Siebert, *$W^{1,\infty}$-convergence of the discrete free boundary for obstacle problems*, IMA J. Numer. Anal., 20 (2000), pp. 481–498.

[20] R. DeVore, *Nonlinear approximation*, Acta Numer.

[21] W. Dörfler, *A convergent adaptive algorithm for Poisson's equation*, SIAM J. Numer. Anal., 33 (1996), 1106–1124.

[22] F. Fierro and A. Veeser, *A posteriori error estimators for regularized total variation of characteristic functions*, SIAM J. Numer. Anal. (to appear).

[23] J. Frehse and U. Mosco, *Irregular obstacles and quasivariational inequalities of stochastic impulse control*, Ann. Scuola Norm. Sup. Cl. Pisa, 9 (1982), pp. 105–157.

[24] A. Friedman, *Variational Principles and Free-Boundary Problems*, Pure Appl. Math., John Wiley, New York, 1982.

[25] D. Gilbarg and N.S. Trudinger, *Elliptic Partial Differential Equations of Second Order*, Springer-Verlag, Germany, 1983.

[26] V. Girault and P.A. Raviart, *Finite Elements for the Navier-Stokes Equations*, Springer (1986)

[27] *GRAPE—GRAphics Programming Environment Manual, Version* 5, SFB 256, University of Bonn, 1995.

[28] V. Grisvard, *Elliptic Problems in Nonsmooth Domains*, Pitman, Boston, 1985.

[29] R. B. Kellogg, *On the Poisson equation with intersecting interfaces*, Appl. Anal., 4 (1975), pp. 101–129.

[30] D. Kinderlehrer and G. Stampacchia, *An Introduction to Variational Inequalities and their Applications*, vol. 88 of Pure Appl. Math., Academic Press, New York, 1980.

[31] I. Kossaczký, *A recursive approach to local mesh refinement in two and three dimensions*, J. Comput. Appl. Math., 55 (1994), pp. 275–288.

[32] K. Mekchay, R.H. Nochetto, *Convergence of adaptive finite element methods for general second order linear elliptico PDE*, SIAM J. Numer. Anal., to appear.

[33] W. Mitchell, *A comparison of adaptive refinement techniques for elliptic problems*, ACM Trans. Math. Software, 15 (1989), pp. 210–227.

[34] P. Morin, R.H. Nochetto, and K.G. Siebert, *Data oscillation and convergence of adaptive FEM*, SIAM J. Numer. Anal., 38, 2 (2000), 466-488.

[35] P. Morin, R.H. Nochetto, and K.G. Siebert, *Convergence of adaptive finite element methods*, SIAM Review, 44 (2002), 631-658.

[36] R. H. Nochetto, *A note on the approximation of free boundaries by finite elements*, RAIRO Model. Math. Anal. Numer., 20 (1986), pp. 355–368.
[37] R.H. Nochetto, *Removing the saturation assumption in a posteriori error analysis*,Istit. Lombardo Sci. Lett. Rend. A, 127 (1993), 67-82.
[38] R. H. Nochetto, *Pointwise a posteriori error estimates for elliptic problems on highly graded meshes*, Math. Comp., 64 (1995), pp. 1–22.
[39] R. H. Nochetto, K. G. Siebert, and A. Veeser, *Pointwise a posteriori error control for elliptic obstacle problems*, Numer. Math., 95 (2003), 163-195.
[40] R. H. Nochetto, K. G. Siebert, and A. Veeser, *Fully localized a posteriori error estimators and barrier sets for contact problems*, SIAM J. Numer. Anal. 42 (2005), 2118-2135.
[41] R. H. Nochetto, L. B. Wahlbin, *Positivity preserving finite element approximation*, Math. Comp. 71 (2001), 1407–1419.
[42] J.-F. Rodrigues, *Obstacle Problems in Mathematical Physics*, vol. 134 of North-Holland Math. Stud., North-Holland, Amsterdam, 1987.
[43] A. Schmidt and K. G. Siebert. *Design of Adaptive Finite Element Software: The Finite Element Toolboox ALBERTA*. LNCSE 42. Springer-Verlag Berlin Heidelberg 2005.
[44] R. Stevenson, *Optimality of a standard adaptive finite element method*, (to appear).
[45] R. Stevenson, *The completion of locally refined simplicial partitions created by bisection*, (to appear).
[46] R. Verfürth, *A Review of A Posteriori Error Estimation and Adaptive Mesh-Refinement Techniques*, Wiley-Teubner, 1995.
[47] A. Veeser, *Efficient and reliable a posteriori error estimators for elliptic obstacle problems*, SIAM J. Numer. Anal., 39 (2001), pp. 146–167.

Ricardo H. Nochetto, Department of Mathematics and Institute of Physical Science and Technology, University of Maryland, College Park, MD 20742, USA.
Partially supported by NSF Grants DMS-0505454.
URL: `http://www.math.umd.edu/~rhn`
E-mail address: `rhn@math.umd.edu`